Ocean Engineering 269 (2023) 113470

Contents lists available at ScienceDirect

Ocean Engineering

journal homepage: www.elsevier.com/locate/oceaneng

Predicting future mooring line tension of floating structure by machine learning

Yu Yang [b], Tao Peng [a,b], Shijun Liao [a,b,*]

[a] State Key Laboratory of Ocean Engineering, Shanghai 200240, China
[b] Center of Marine Numerical Experiment, School of Naval Architecture, Ocean and Civil Engineering, Shanghai Jiao Tong University, Shanghai 200240, China

ARTICLE INFO

Keywords:
Mooring tension
Barge
KVLCC2 ship
Irregular wave
Machine learning

ABSTRACT

The prediction of mooring line tension is helpful for the station-keeping of floating structures. In this study, we propose a machine learning approach based on the reservoir computing (RC) model to predict the mooring line tension of a barge and the KVLCC2 ship, respectively. The datasets were collected from the model tests carried out in the deep-water wave basin. The RC model was trained using the low-frequency and wave-frequency parts of the mooring line tension combined with its main relevant vessel motion. The prediction was obtained by superposing these two components of tension. Finally, the trained model could extend the predictions of mooring line tension 80 s into the future with high accuracy, which was validated by the corresponding experimental results. This strategy has been verified to improve the prediction accuracy significantly. Besides, compared with the long short-term memory (LSTM) model, the RC model was found to be more accurate and efficient to predict the mooring line tension. This work provides some guidelines and shows the great potential of the proposed method to forecast mooring tensions for offshore vessels and platforms.

1. Introduction

Mooring systems (Ma et al., 2019; Xiao et al., 2014) are used to provide stability for floating platforms or vessels against the sea states. The mooring systems are essential to ensure the safety of many operations conducted on floating structures. The failure of a mooring system can lead to serious environmental and economic damage. The ability to predict mooring line tension can be combined with machine learning techniques (Rezaniaiee Aqdam et al., 2018; Janas et al., 2021) and sensors (De Girolamo et al., 2019) to enable the development of new applications, such as the forecast and detection of mooring failure, the early warning information system, as well as the active mooring line tension control. Thus, predicting offshore mooring line tension is meaningful, which contributes a lot to enhancing the reliability and safety of the mooring system and the overall floating system at the operational stage of floating structure. For such cases of application, the model ought to be able to use existing data from sensors for accurate predictions of mooring line tensions.

Numerical simulation is often used to explore the field of ocean engineering (Yan et al., 2020; Li et al., 2021b; Yang and Li, 2022). In recent years, machine learning (ML) technique (Mitchell and Mitchell, 1997; Jordan and Mitchell, 2015; Li et al., 2021a) has been explored a lot and successfully applied in offshore engineering. It provides us with an effective framework to study features directly from the data without much knowledge related to underlying physics. (Sclavounos and Ma, 2018) employed the support vector machine model to predict a wave in a short term. The backpropagation (BP) neural network has been used to study the fatigue behavior of the catenary riser (Quéau et al., 2014). Mak and Düz (2019) used the machine learning approach to estimate the relative wave direction based on the time histories of ship motions. Kim (2015) applied the NARX (Nonlinear Autoregressive with Exogenous Input) neural network to predict the response of a slender marine structure under an irregular wave based on the Volterra series. Liong and Chua (2022) developed a data assimilation framework based on the artificial neural network (ANN) for deterministic prediction of vessel motion in real-time. The long short-term memory (LSTM) network (Guo et al., 2021, 2022) has been used to predict the motions of a semi-submersible. The Bi-LSTM and encoder–decoder LSTM have been employed to predict the tide level and storm surge, respectively (Bai and Xu, 2022, 2021). Chaves et al. (2015) combined the dynamic finite element analysis and the ANN to the fatigue calculations of flexible pipes.

There are some successful applications of monitoring the mooring line tensions based on the vessel motions, by using the ML techniques. When the ML model has been trained, it can be efficiently applied to model the relationship between the mooring line tensions and vessel motions and predict the mooring line tensions based on the motion

* Corresponding author at: State Key Laboratory of Ocean Engineering, Shanghai 200240, China.
E-mail address: sjliao@sjtu.edu.cn (S. Liao).

https://doi.org/10.1016/j.oceaneng.2022.113470
Received 15 September 2022; Received in revised form 26 November 2022; Accepted 18 December 2022
Available online 29 December 2022
0029-8018/© 2022 Elsevier Ltd. All rights reserved.

Table 1
The main dimensions and parameters of the rectangular barge.

Parameter	Unit	Prototype	Model
Hull length	m	213.312	3.333
Hull width	m	49.088	0.767
Hull height	m	27.2	0.425
Draught	m	11.84	0.185
Displacement	t	123520.29	0.4597
Vertical center of gravity	m	17.344	0.271
Longitudinal Center of Gravity	m	106.688	1.667
Roll gyradius	m	15.808	0.247
Pitch gyradius	m	67.84	1.06

responses. Christiansen et al. (2015) applied a hybrid method based on the ANN to predict the current mooring line tension. The input data included the six degrees of freedom motion and the previous mooring line tension. Sidarta et al. (2017) applied an ANN to predict the mooring line tensions using the ship motions as the input data. Kumar et al. (2020) successfully predicted the mooring line tensions based on the fairlead motion by separating low-frequency and wave-frequency components of tensions such that the former was approximated as quasi-static tensions and the latter was predicted by the ANN. Based on the LSTM neural network, Qiao et al. (2021) and Wang et al. (2022) accurately predicted the mooring line tension from the vessel motion, where the inputs were the motions and the outputs were corresponding mooring line tension responses. Note that, rather than predicting the present mooring line tension based on vessel motion, in this study, we try to make future predictions of the mooring line tension based on the existing data of mooring line tension and vessel motion. This has significant meanings related to early-warning information, forecast and detection of mooring line failure, active tension control, etc.

The recurrent neural networks (RNNs) (Mandic and Chambers, 2001; Mikolov et al., 2010) are effective ML techniques, which have been successfully applied in the field of sequential data processing. The frameworks of RNNs combine the temporal dependence of the input with the historical system dynamics. In recent years, it has been demonstrated that a ML model known as reservoir computing (RC) had great performance in modeling and predicting many complex dynamical systems (Jaeger and Haas, 2004; Pathak et al., 2017; Lu et al., 2018; Nakai and Saiki, 2018; Pathak et al., 2018; Jiang and Lai, 2019; Tanaka et al., 2019; Vlachas et al., 2020). The RC model has also been successfully used to predict the motions of a moored vessel in irregular waves, which was purely based on the motion data (Yang et al., 2022). The framework of the RC model comes from the RNN, and thus it is suitable for sequential information processing. The low-dimensional input is put into a high-dimensional phase space called a reservoir. The neural network weights inside the reservoir are specified through an adjacency matrix. This matrix is a sparse random matrix, and its elements are not trained. The readout weights are trained to map the reservoir state to the target output. The training process does not rely on the backpropagation algorithm to determine the weights inside the model, and only the weights in the output layer are trainable. Therefore, compared with the standard RNN and the LSTM network, the RC model can alleviate the difficulty of learning the recurrent connections and decrease the training cost (Vlachas et al., 2020).

The objective of this paper is to introduce the application of machine learning based on the RC model to predict mooring line tension into the future. The RC model is trained based on the low-frequency and wave-frequency parts of mooring line tension combined with its main relevant vessel motion. The rectangular barge and the KVLCC2, which have obviously different frame lines, were used as two cases to test the performances of different ML models. (The full name of KVLCC2 is KRISO (Korean Institute of Ships and Ocean Engineering) Very Large Crude Carrier no.2.) The proposed method could provide the predictions of mooring line tension 80 s into the future with high accuracy, which was validated by the corresponding experimental results. Besides, this strategy has been verified to improve the prediction accuracy significantly. In addition, the RC model was found to be more accurate and efficient than the LSTM model to predict mooring line tension. In general, the work provides some guidelines and shows the great potential of this method to predict mooring tensions for offshore vessels and platforms.

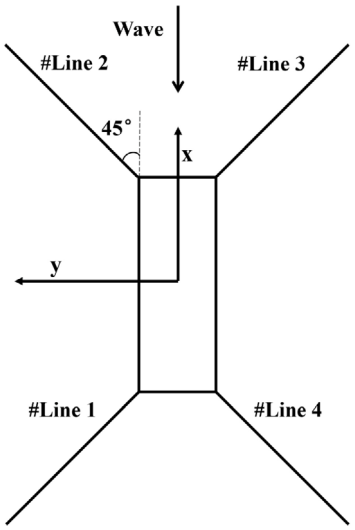

Fig. 1. Sketch map of the mooring system for the rectangular barge in the wave basin.

The rest of the paper is structured as follows. In Section 2, we illustrate the model tests of a moored rectangular barge and the KVLCC2 ship in irregular waves, respectively, which generated the datasets for training and testing the ML models. In Section 3, the basic structure of the RC model is described. Then, the training processes of RC models to predict mooring tension based on three different strategies are illustrated. Besides, the determination of the optimal hyper-parameters of the RC model is illustrated. In Section 4, the performances of models based on different strategies are evaluated and compared. Besides, the performance of the RC model is compared with the LSTM model results based on the proposed method. Finally, Section 5 describes the concluding remarks and discussions.

2. Experiment

In this section, we describe the scaled model tests carried out in the deep-water basin at Shanghai Jiao Tong University (SJTU), China. A moored barge and a moored KVLCC2 ship were tested in irregular waves, respectively. The length and width of this deep-water basin were 50.0 m and 40.0 m, respectively. During the model tests, the water depth was 8 m. A wave maker was used to model ocean waves. Next, the model tests are illustrated from three aspects, including the model and mooring system, the irregular wave simulation, and the data collection and analysis.

2.1. Rectangular barge

2.1.1. Model and mooring system

First, we consider a model test of the moored rectangular barge in the irregular wave environment. Table 1 illustrates the main properties and dimensions of this rectangular barge model. The scaled ratio of the barge was 1: 64. The corresponding water depth in the prototype was 512 m. During the model test, the barge model was moored in the horizontal soft mooring system. As shown in Fig. 1, the barge model was moored by the four horizontal mooring lines that were attached to the corners. The angle between each line and the x direction of the

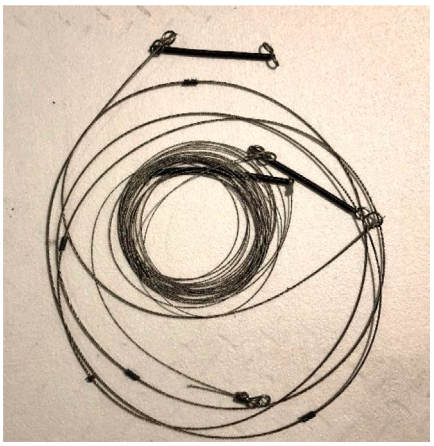

Fig. 2. The mooring line used in the model test.

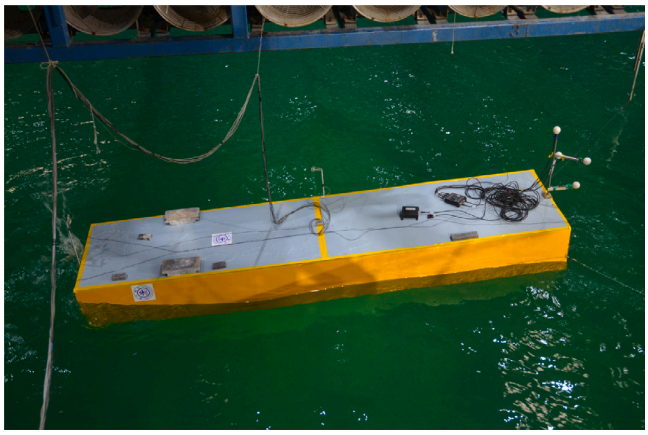

Fig. 4. The barge model tested in irregular waves.

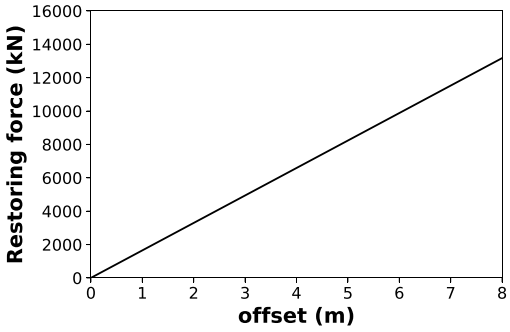

Fig. 3. Static offset curve in surge direction for the model test of barge.

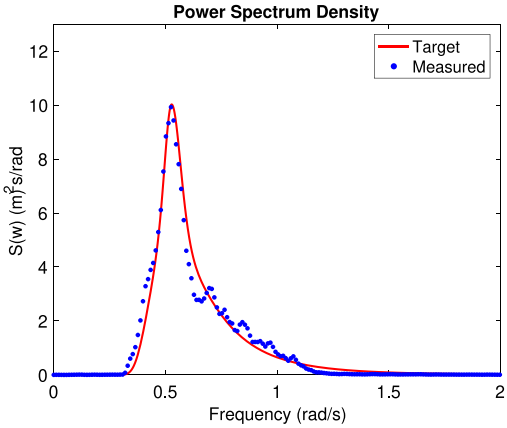

Fig. 5. Power spectrum density of the wave calibration compared with the target JONSWAP wave result for the model test of the barge.

coordinate system was 45°. The used mooring line is shown in Fig. 2, which was made by the wire rope and the spring. To capture the six degrees of freedom (DoF) motions, an optical motion capture system was applied. The four mooring line tensions were measured by the tension sensors. The natural periods of the surge, heave, and pitch motions were measured to be 58.51 s, 10.40 s, and 11.56 s, respectively. The center point of the rectangular barge on the baseline was defined as the origin (0, 0, 0) of the coordinate. The x and y axes are shown in Fig. 1, and the z axis was perpendicular to the x–y plane. Then, the fairlead positions were (−106.67, 24.54, 11.84), (106.67, 24.54, 11.84), (106.67, −24.54, 11.84), and (106.67, −24.54, 11.84), respectively. The anchor positions were (−219.80, 137.68, 11.84), (219.80, 137.68, 11.84), (−219.80, −137.68, 11.84), and (219.80, −137.68, 11.84), respectively. The static offset curve in the surge direction from the experiment is shown in Fig. 3. The stiffness of the spring was 885.5 kN/m, and the pre-tension was 3449.0 kN. Fig. 4 shows the moored rectangular barge tested in the wave basin.

2.1.2. Irregular wave simulation

The irregular waves were generated following the JONSWAP spectrum as,

$$S(f) = \alpha H_s^2 T_p^{-4} f^{-5} exp[-1.25(T_p f)^{-4}] \gamma^{exp[-\frac{(T_p f-1)^2}{2\sigma^2}]}, \quad (1)$$

where $F_p = 1/T_p$ is the spectral peak frequency, T_p is the spectral peak period, H_s is the significant wave height, $\sigma = 0.09$ when $f > F_p$, and $\sigma = 0.07$ when $f < F_p$, and α is related to shape parameter γ, i.e.

$$\alpha = \frac{0.0624}{0.230 + 0.0336\gamma - 0.185/(1.9 + \gamma)}. \quad (2)$$

The shape parameter γ was 2. The target significant wave height H_s was 6.0 m, and the target spectral peak period T_p was 11.9 s. Note that, to better test the performance of the ML model, the wave parameters were chosen with the consideration that the sea state was rather rough, so the responses of the mooring line tension were quite intense. The ability to make predictions of mooring line tension when the variation in tension is intense can be more significant and meaningful. The irregular wave direction was 180° as shown in Fig. 1. The wave elevations were calibrated before the model test started. Fig. 5 presents the power spectrum density of measured wave elevation compared with the target result. Table 2 illustrates the spectral analysis of the irregular wave simulation. The acceptance criterion was that the differences between the measured values (significant wave height and spectral peak period) and the corresponding target values were both less than 5%. It is shown that the differences between the measured values and target values were both less than 0.34%. Thus, the irregular wave simulation met the acceptance criterion.

Table 2
Comparison of the measured value and target value of the irregular waves for the model test of the barge.

Parameters	Unit	Measured value	Target value
Significant wave height	m	6.02	6.00
Spectrum peak period	s	11.90	11.90
Peak value of spectrum	m^2 s/rad	11.49	11.36

2.1.3. Data collection and analysis

After the wave calibration, the barge model was put into the basin and moored by the mooring system. Then, the irregular waves were

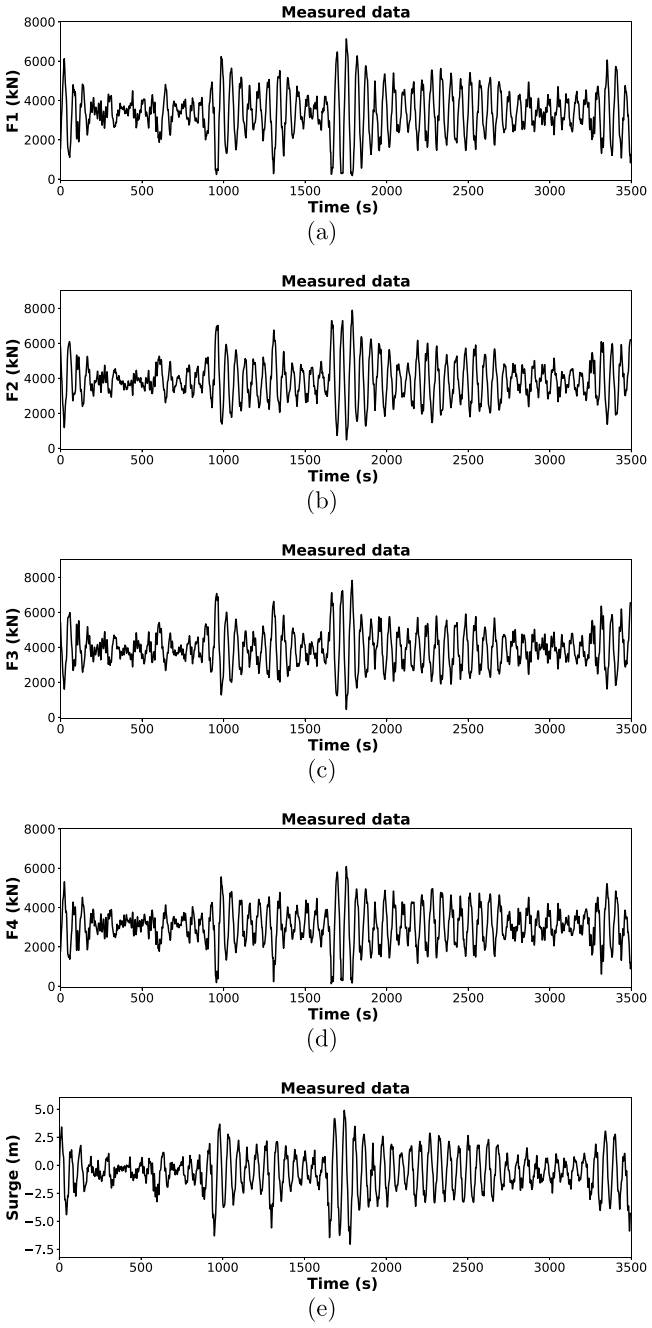

Fig. 6. The time histories of four mooring line tensions and surge motion of the rectangular barge from the model test.

generated, and mooring line tensions and motions were synchronously recorded for more than 30 min, which corresponds to 3 h in the prototype. The sampling frequency was 25 Hz, corresponding to 3.125 Hz in the prototype. Finally, the model test of the moored barge generated a dataset consisting of 43000 sample points, i.e. 13760 s. The mooring tensions of the lines 1, 2, 3, and 4 are denoted as F_1, F_2, F_3, and F_4, respectively. The time series of four mooring tensions and surge motion are shown in Fig. 6. The statistics of the tensions of four mooring lines and surge motion in the time domain are listed in Table 3, including the maximum, minimum, and mean values, standard deviation (Std.), significant positive single amplitude (Pos.Sign.), significant negative single amplitude (Neg.Sign.), and significant double amplitude (Dou.Sign.).

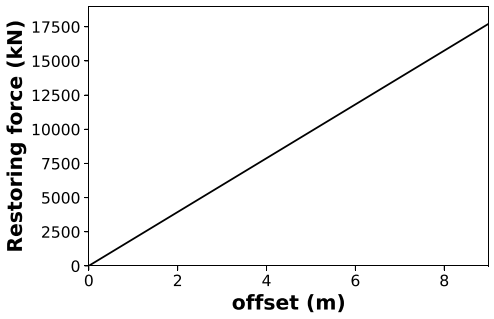

Fig. 7. Static offset curve in surge direction for the model test of the KVLCC2 ship.

Fig. 8. The KVLCC2 ship model tested in irregular waves.

2.2. KVLCC2 ship

2.2.1. Model and mooring system

Another model test of a different vessel type was also carried out in the deep wave basin. The scaled KVLCC2 ship model was tested in irregular waves. The scale ratio was set to be $\lambda = 1 : 70$. The water depth in the prototype was 560 m. The main parameters of the KVLCC2 ship are described in Table 4. The horizontal mooring system consisted of four mooring lines, which were the same as those used in the model test of the rectangular barge described in Section 2.1.1. The natural periods of the surge, heave, and pitch motions were measured to be 78.10 s, 10.98 s, and 10.69 s, respectively. The center point of the vessel on the baseline was defined as the original (0, 0, 0). Then, the fairlead positions were (−121.42, 25.92, 30), (121.42, 26.88, 30), (121.42, −26.88, 30), and (−121.42, −25.92, 30), respectively. The anchor positions were (−245.16, 149.66, 30), (245.16, 150.62, 30), (245.16, −150.62, 30), and (−245.16, −149.66, 30), respectively. The static offset curve in the surge direction from the experiment is shown in Fig. 7. The stiffness of the spring was 1059.3 kN/m, and the pre-tension was 3449.0 kN. The KVLCC2 ship model tested in the deep-water basin is shown in Fig. 8.

2.2.2. Irregular wave simulation

The irregular wave simulation was also generated following the JONSWAP spectrum as in Eq. (1) with shape parameter γ set to 2. The target significant wave height H_s was 10.90 m, and the target spectral peak period T_p was 12.50 s. The irregular wave direction was 180°. Fig. 9 presents the power spectrum density of measured wave elevation compared with the target result. Table 5 illustrates the spectral analysis of the irregular wave simulation. It is shown that the differences between the measured values (significant wave height and peak spectral period) and the corresponding target values were less than 1.2%. Thus, the irregular wave simulation met the acceptance criterion.

Table 3
Statistics of the time domain of the mooring line tensions for the rectangular barge from the model test in the prototype.

Title	Unit	Max	Min	Mean	Std.	Pos.Sign.	Neg.Sign.	Dou.Sign.
F_1	kN	7052.91	38.09	3293.46	998.53	1918.13	−1976.3	3816.70
F_2	kN	8171.77	362.83	3905.36	1004.94	2015.77	−1894.02	3803.12
F_3	kN	7827.53	446.17	3951.07	916.86	1833.21	−1683.58	3419.50
F_4	kN	6004.68	24.92	2998.29	834.39	1567.04	−1634.45	3101.61
Surge	m	4.8954	−7.4432	−0.6266	1.5479	2.9092	−3.1449	5.8896

Table 4
Main dimensions and parameters for the KVLCC2 ship.

Particulars	Unit	Actual value	Model value
Hull length	m	320	4.571
Hull width	m	58	0.829
Hull height	m	30	0.429
Draught	m	20.8	0.297
Displacement	t	320438	0.9114
Vertical center of gravity	m	18.6	0.266
Longitudinal center of gravity	m	11.1	0.159
Roll gyradius	m	23.2	0.331
Pitch gyradius	m	80	1.143

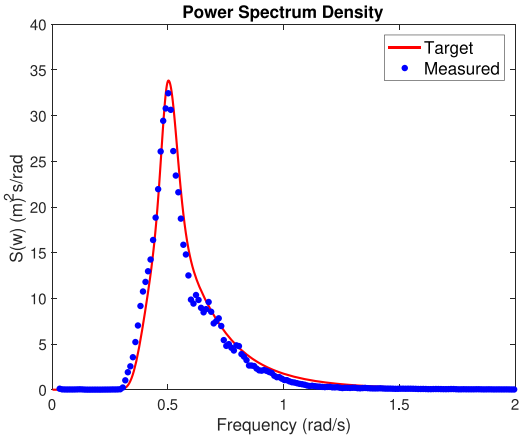

Fig. 9. Power spectrum density of the wave calibration compared with the target JONSWAP wave result for the model test of the KVLCC2 ship.

Table 5
Comparison of the measured value and target value of the irregular waves in the model test of the KVLCC2 ship.

Parameters	Unit	Measured values	Target values
Significant wave height	m	10.77	10.90
Spectrum peak period	s	12.44	12.50
Peak value of spectrum	m^2 s/rad	37.41	33.80

2.2.3. Data collection and analysis

In the model test of the moored KVLCC2 ship, the sampling frequency was 25 Hz, corresponding to 2.988 Hz in the prototype. The dataset consisted of 43000 sample points, corresponding to 14391 s in the prototype. The time histories of the four mooring tensions and surge motion are shown in Fig. 10. The statistics of the tensions of four mooring lines and surge motion in the time domain are listed in Table 6, including the maximum, minimum, and mean values, standard deviation (Std.), significant positive single amplitude (Pos.Sign.), significant negative single amplitude (Neg.Sign.), and significant double amplitude (Dou.Sign.).

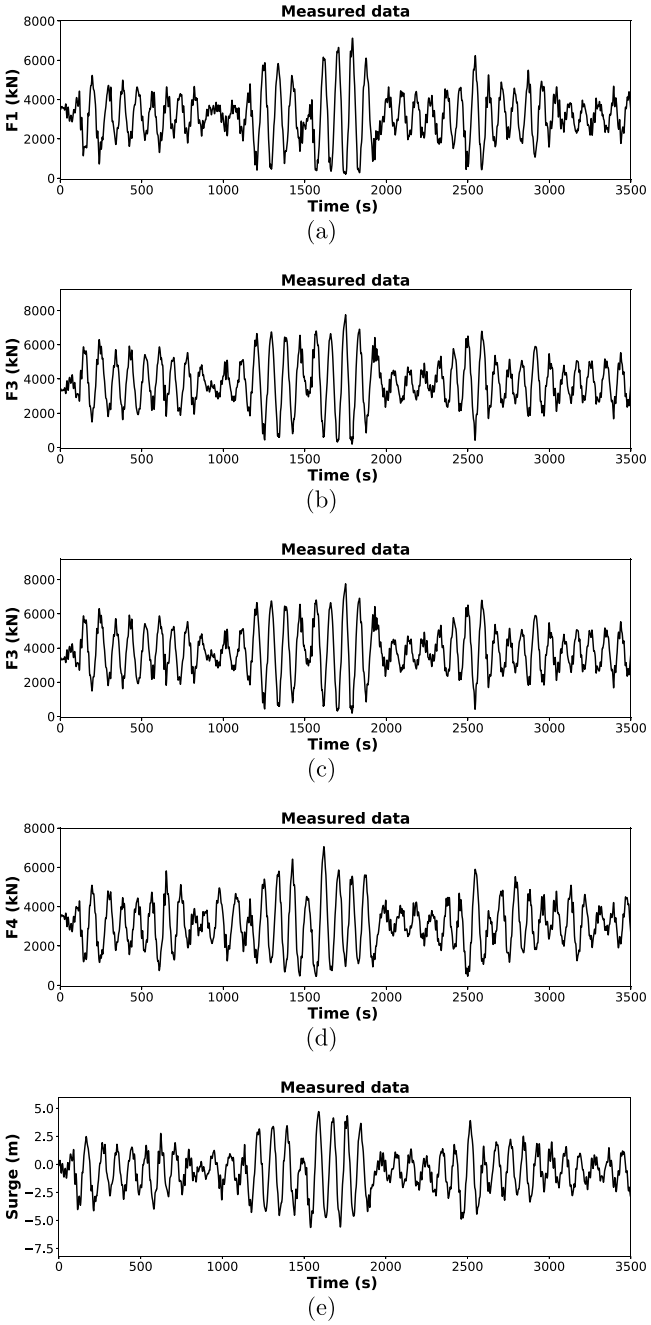

Fig. 10. The time histories of four mooring line tensions and surge motion of the KVLCC2 ship from the model test.

3. Methodology

In this section, the proposed approach based on the RC model to predict future mooring line tensions of vessel will be illustrated in the following aspects. First, we briefly introduce the main structure of the RC model in Section 3.1. Then, the training processes based on the RC model are illustrated in Section 3.2. Three strategies for training are taken into consideration. Next, the data preprocessing and the divisions of the dataset into the training set, validation set, and test set are described in Section 3.3. Besides, the evaluation indexes used

Table 6
Statistics of the time domain of the mooring line tensions for the KVLCC2 ship from the model test in the prototype.

Title	Unit	Max	Min	Mean	Std.	Pos.Sign.	Neg.Sign.	Dou.Sign.
F_1	kN	7730.85	67.26	3078.51	1345.21	2670.11	−2542.08	5130.56
F_2	kN	8684.52	444.21	3971.56	1420.82	2799.48	−2712.71	5392.59
F_3	kN	9761.52	51.74	3857.05	1759.54	3545.67	−3410.72	6906.81
F_4	kN	8190.12	132.27	3018.62	1540.59	3243.00	−2616.35	5774.38
Surge	m	6.3073	−8.2443	−0.6584	2.263	4.4515	−4.477	8.8061

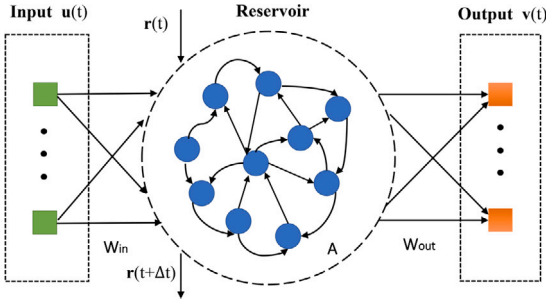

Fig. 11. The framework of reservoir computing (RC) model.

for evaluating the predictions are shown in Section 3.4. In addition, the determination of optimal hyper-parameters of the RC model is illustrated in Section 3.5. The influence of the hyper-parameters of the RC model on the prediction performance is illustrated.

3.1. Reservoir computing model

In this section, we introduce the main structure of a machine learning technique named the reservoir computing (RC) model. The RC model has been successfully applied to predict many complex dynamical systems (Jaeger and Haas, 2004; Pathak et al., 2017; Lu et al., 2018; Nakai and Saiki, 2018; Pathak et al., 2018; Jiang and Lai, 2019; Tanaka et al., 2019; Vlachas et al., 2020). The input vector $\mathbf{u}(t)$ with dimension D_{in} is fed to a middle layer called "reservoir" with dimension D_r via an input-to-reservoir coupler. The output vector $\mathbf{v}(t)$ with dimension D_{out} is generated from the reservoir via a reservoir-to-output coupler. The general structure is shown in Fig. 11. The reservoir is a low-degree (κ), sparse and random network, consisting of a $D_r \times D_r$ adjacency matrix $\mathbf{A}$. Inside the matrix $\mathbf{A}$, the elements are generated from the uniform distribution in $[0, \alpha]$, where α is determined as the largest eigenvalue of $\mathbf{A}$ is equal to the target value ρ referring to the spectral radius of the reservoir. The functions of input-to-reservoir coupler can be presented in discrete time ($t = 0, \Delta t, 2\Delta t, \ldots, N_{t-1}\Delta t$), given by Pathak et al. (2017, 2018)

$$\mathbf{r}(t + \Delta t) = \tanh[\mathbf{A}\mathbf{r}(t) + \mathbf{W}_{in}\mathbf{u}(t)], \tag{3}$$

and the functions of the reservoir-to-output coupler can be described as

$$\mathbf{v}(t + \Delta t) = \mathbf{W}_{out}(\mathbf{r}(t + \Delta t), \mathbf{P}), \tag{4}$$

where $\mathbf{r}(t)$ denotes the scalar states $r_i(t)$ (i = 1, 2, …, D_r) of reservoir nodes; the matrix $\mathbf{W}_{in}$ with $D_r \times D_{in}$ dimensions maps the input vector $\mathbf{u}(t)$ to the reservoir state $\mathbf{r}(t)$; the matrix $\mathbf{W}_{out}$ with $D_{out} \times D_r$ dimensions maps $\mathbf{r}(t)$ to the output vector $\mathbf{v}(t)$. The elements of the $\mathbf{W}_{in}$ are chosen from the uniform distribution in $[-\sigma, \sigma]$, and each reservoir node receives a scalar input from $\mathbf{u}(t)$. The $\mathbf{W}_{out}$ relies on adjustable parameters of the $\mathbf{P}$. Here, $\mathbf{W}_{out}$ is defined as $\mathbf{W}_{out}(\mathbf{r}) = \mathbf{P}_1\mathbf{r} + \mathbf{P}_2\mathbf{r}^2$, where $\mathbf{P} = (\mathbf{P}_1, \mathbf{P}_2)$ (Pathak et al., 2018).

In the training phase ($t = 0, \Delta t, 2\Delta t, \ldots, N_{t-1}\Delta t$) with all N_t timesteps, the initial reservoir state is $\mathbf{r}(0) = 0$. The reservoir state $\mathbf{r}(t)$ is updated at every timestep Δt according to Eq. (3) by involving the $(N_t - 1)$ timesteps of input $\mathbf{u}(t)$ in $t = 0, \Delta t, \ldots, N_{t-2}\Delta t$. Then we get the reservoir state $\mathbf{r}(t)$ at $t = \Delta t, 2\Delta t, \ldots, N_{t-1}\Delta t$. We disregard the first τ steps of the reservoir state $\mathbf{r}(t)$ as transients (Vlachas et al., 2020; Jiang and Lai, 2019). The output $\mathbf{v}(t)$ at $t = (S + 1)\Delta t, \ldots, N_{t-1}\Delta t$ is then obtained by Eq. (4). To make the $\mathbf{v}(t)$ approximate the target result $\mathbf{v}_d(t)$, the output parameters $\mathbf{P}$ are determined to minimize the difference between $\mathbf{v}(t)$ and $\mathbf{v}_d(t)$.

The regularized regression (Tikhonov and Arsenin, 1977) is applied to obtain the output matrix $\mathbf{P}$, by minimizing the following function

$$\sum_{t=(\tau+1)\Delta t}^{N_{t-1}\Delta t} \| \mathbf{W}_{out}(\mathbf{r}(t), \mathbf{P}) - \mathbf{v}_d(t) \|^2 + \beta \| \mathbf{P} \|^2, \tag{5}$$

where parameter $\beta > 0$ is applied to discourage overfitting through penalizing large output weights.

In the prediction phase, if one wants to forecast $\mathbf{u}(t)$ for $t > t_0$, the reservoir state $\mathbf{r}(t_0)$ can be obtained by Eq. (3) for the time $\tau\Delta t$ before t_0 i.e., $(t_0 - \tau\Delta t \le t \le t_0)$, where $\mathbf{r}(t_0 - \tau\Delta t) = 0$. Then the RC model can be applied to predict time series for $t > t_0$ by iteratively using the following equation

$$\mathbf{r}(t + \Delta t) = \tanh[\mathbf{A}\mathbf{r}(t) + \mathbf{W}_{in}\mathbf{W}_{out}(\mathbf{r}(t))]. \tag{6}$$

Then, the predictions are given by

$$\mathbf{v}(t) = \mathbf{W}_{out}(\mathbf{r}(t)). \tag{7}$$

3.2. Training process

Here, we illustrate the training process based on the RC model for predicting future mooring line tension.

A simple thought of predicting future mooring tension is to train the RC model purely based on the past mooring line tension data, and we tried this strategy as a preliminary attempt. Besides, as the mooring line tension is closely related to the vessel motion, including more relevant data to train the model may help it better learn the underlying features and improve its performance. Therefore, we combined the mooring line tension with the main relevant vessel motion to train the RC model and tested its performance. As the barge and the KVLCC2 ship were tested in the irregular head waves, the mooring tensions were mainly affected by surge motion. The surge motion was combined with the mooring tension data to train the RC model. Note that, to predict the mooring line tension based on the vessel motion, Kumar et al. (2020) successfully employed the ANN to predict the tensions by separating low-frequency and wave-frequency components of tensions. Besides, using the vessel motion as input, Wang et al. (2022) illustrated that the LSTM model based on the divided low-frequency and wave-frequency parts of tension and vessel motion could better predict the present mooring line tension, compared with the LSTM model trained based on the global responses. Therefore, as motivated by their works, we investigated the performance of the RC model to predict future mooring line tension based on the low-frequency and wave-frequency parts of the mooring line tension and surge motion.

From the model tests, the power spectrum densities of the mooring line tensions (F_1 and F_2) and the surge motion are presented in Fig. 12 for the barge case and in Fig. 13 for the KVLCC2 ship case. It is shown that the mooring line tensions and surge motion responses mainly consist of two parts: the low-frequency part and the wave-frequency part. The low-frequency component is much larger compared with the wave-frequency component. The peak spectrum frequency of the

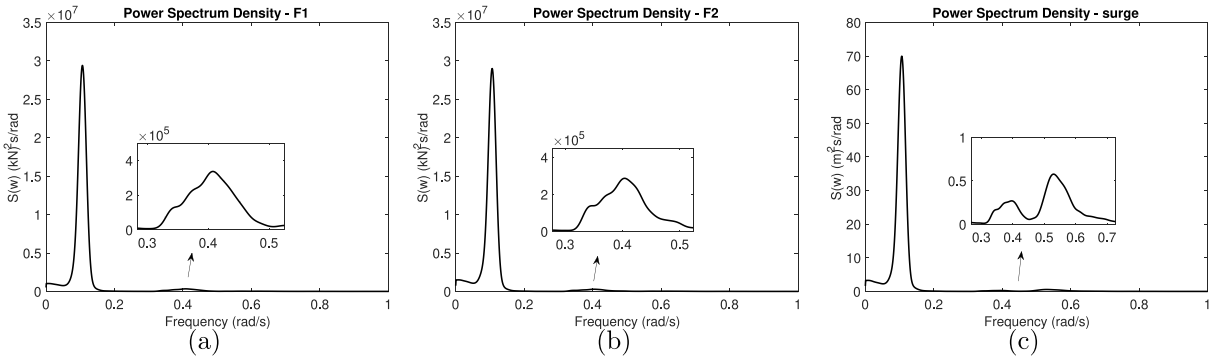

Fig. 12. Power spectrum density of mooring line tensions F_1 (a), F_2 (b) and surge motion (c) from the model test of the rectangular barge.

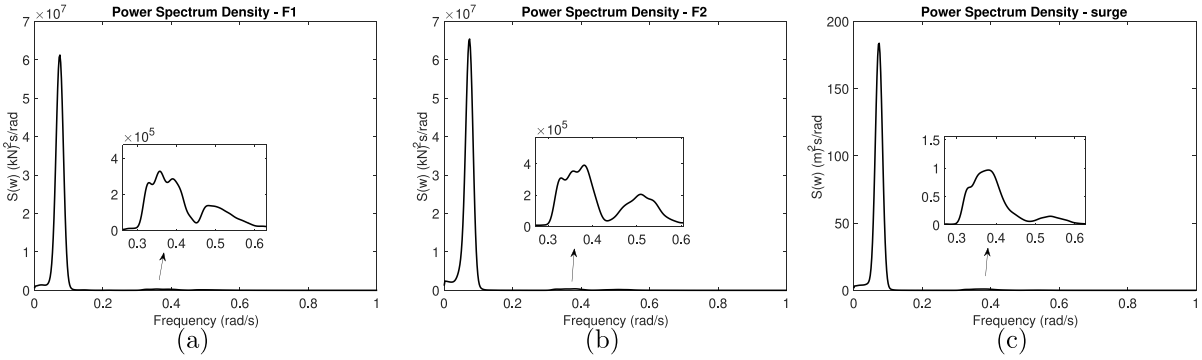

Fig. 13. Power spectrum density of mooring line tensions F_1 (a), F_2 (b) and surge motion (c) from the model test of the KVLCC2 ship.

Table 7
Three different strategies based on the RC model to predict the future mooring line tension.

Strategy	Training process
A	The RC model was trained purely based on the global responses of mooring line tension data.
B	The RC model was trained based on the global responses of tension combined with the surge motion data.
C	The RC model consisted of two sub-RC models. One was trained based on the low-frequency parts of mooring line tensions and surge motion, and the other one was trained based on the corresponding wave-frequency parts of tension and surge data. Finally, the mooring line tension was predicted by the superposition of low-frequency tension and wave-frequency tension.

surge is close to the mooring line tensions. The low-frequency parts of mooring line tensions and surge could be separated by a low-pass filter with the cut-off frequency of 0.3 rad/s ($\omega < 0.3$ rad/s). The global response minus the low-frequency part gave the corresponding wave-frequency part ($\omega > 0.3$ rad/s). Then, we define these three different strategies mentioned above to predict the mooring line tension in Table 7. To investigate whether including the main relevant vessel motion into the dataset and using the divided components to train the RC model are necessary, the performances of these three strategies will be compared in Section 4.

3.3. Dataset and data preprocessing

The dataset was collected from the model test with 43000 sample points. The first 34000 samples were used as the training data for the RC model. To determine the hyper-parameters of the RC model, the next 1000 samples were applied as the validation set. The last 8000 samples were used as the test set to evaluate the performance of the trained model. The divisions of datasets in the prototypes for the barge and the KVLCC2 ship are listed in Table 8, respectively. For strategy A, the model was constructed only based on the mooring line tensions. For strategies B and C, the dataset contained the mooring line tensions and surge motion.

First, data preprocessing was performed before we used the data to train the RC model. The data have different characteristics, as the mooring line tensions are measured in kN while the surge motion is measured in meters, and the magnitudes of the tensions and surge motion are also different. Therefore, the data were normalized to eliminate the dimension influence and maintain accuracy during the training process. Each data was normalized as follows,

$$\tilde{x}_i(t) = \frac{x(t_i) - a}{b - a}, \tag{8}$$

where a and b are the minimum and maximum values of the training dataset, respectively. Finally, the outputs were scaled up to give the results.

3.4. Evaluation index

The performance of ML prediction was evaluated by comparing the outputs with the corresponding experimental results. In this work, three kinds of indicators were used to evaluate the performance of prediction, including the normalized mean absolute error E_{abs}, the extreme value error E_{max}, and the curve fitting degree R_{new}. The evaluation indexes are defined as follows,

$$E_{abs} = \frac{1}{n}\sum_{i=1}^{n}\frac{|y_i^{true} - y_i^{pred}|}{\bar{y}_{true}}, \tag{9}$$

$$E_{max} = \left|\frac{y_{true}^{max} - y_{pred}^{max}}{y_{true}^{max}}\right|, \tag{10}$$

$$R_{new} = 1 - \sqrt{\frac{\sum_{i=1}^{n}(y_i^{true} - y_i^{pred})^2}{\sum_{i=1}^{n}(y_i^{true})^2}}, \tag{11}$$

Table 8
Divisions of datasets from the model tests of the barge and the KVLCC2 ship.

Type	Sample frequency	Time step	Training set	Validation set	Test set
Rectangular barge	3.125 Hz	0.320 s	34000 points $t \in [0, 10880]$ s	1000 points $t \in [10880, 11200]$ s	8000 points $t \in [11200, 13760]$ s
KVLCC2 ship	2.988 Hz	0.335 s	34000 points $t \in [0, 11379]$ s	1000 points $t \in [11379, 11714]$ s	8000 points $t \in [11714, 14391]$ s

Table 9
Optimal hyper-parameters of the RC model for predicting the mooring line tensions of the barge.

Barge	ρ	σ	β	D_r	τ	κ
Strategy A	0.9	10^{-7}	0	3000	80	3
Strategy B	0.9	10^{-7}	0	3000	80	3
Strategy C	0.7	10^{-8}	0	3000	80	3

Table 10
Optimal hyper-parameters of the RC model for predicting the mooring line tensions of the KVLCC2 ship.

KVLCC2 ship	ρ	σ	β	D_r	τ	κ
Strategy A	0.9	10^{-5}	0	3000	80	3
Strategy B	0.9	10^{-6}	0	3000	80	3
Strategy C	0.8	10^{-5}	0	3000	80	3

where y_i^{true} is the measured data from the experiment, y_i^{pred} is the prediction given by the ML model, $\bar{y}_{true}$ is the mean value of actual mooring line tension, y_{true}^{max} is the maximum value of actual mooring line tension, y_{pred}^{max} is the maximum value of prediction, and n is the prediction length. When the predictions match the actual values, the indexes E_{abs} and E_{max} are close to 0, while the index R_{new} is close to 1. Here, the evaluation indexes are defined for one test set with a prediction length n. The evaluation indexes across different test sets are defined as the corresponding mean values of the indexes over different test sets.

3.5. Determination of optimal model hyper-parameters

In this section, we consider determining the hyper-parameters of the RC models to predict the mooring line tensions of the rectangular barge and the KVLCC2 ship, respectively. As illustrated in Section 3.1, the number of samples used to train the RC model was $N_t = 34000$ for the three strategies. The neuron nodes inside the reservoir D_r and the degree ϵ of the random network were first chosen as $D_r = 3000$ and $\epsilon = 3$. The grid search was carried out to determine the hyper-parameters $(\rho, \sigma, \beta, \tau)$ of the RC model by evaluating the mooring tension predictions from 16 different initial conditions in the validation set with the prediction length of 60 s, where the hyper-parameter ρ refers to the spectral radius of the reservoir, the σ is the input weight scaling factor, the β represents the regularization parameter to prevent overfitting, and τ is the length of actual measurements before the prediction start time to warm up the state of the RC model.

The initial conditions were uniformly distributed with a time interval of 50 timesteps. The hyper-parameters of ρ, σ and β were determined as the model had the smallest normalized mean absolute error E_{abs} in the validation set. The parameter τ was determined by increasing the value of τ until there was almost no further improvement in the prediction performance. As the optimal hyper-parameters for different strategies might not be the same, they were determined for different strategies, respectively. The hyper-parameters are shown in Table 9 for the case of the rectangular barge. As for the case study of the KVLCC2 ship, the optimal hyper-parameters of the RC models based on different strategies were chosen in a similar way, as illustrated in Table 10.

The influences of the model parameters $(\rho, \sigma, \beta, \tau)$ on the prediction quality are presented in Fig. 14 by evaluating the error E_{abs} in the validation set for the case studies of the barge and the KVLCC2 ship, respectively. When varying one parameter, other parameters stayed the same. It is shown that when $\rho \leq 0.7$, the error decreased slightly as the spectral radius ρ of the reservoir increased. The error varied slightly as σ changed from 10^{-8} to 10^{-5}. The error increased in general as the value of the regularization parameter β increased. Besides, as shown in Fig. 14, the error remained almost unchanged when the length of time step τ was greater than 80. Thus, the 80 time steps of true measurements before the prediction start time were enough to warm up the state of the RC model for future predictions. As illustrated in Section 3.1, to make predictions for $t > t_0$, $\tau = 80$ timesteps of true measurements (i.e. $t_0 - 80\Delta t \leq t \leq t_0$) were used to obtain the reservoir state $\mathbf{r}(t_0)$ at the prediction start time t_0 through Eq. (3) with the reservoir's initial state $\mathbf{r}(t_0 - 80\Delta t) = \mathbf{0}$. The reservoir state $\mathbf{r}(t_0)$ could then be used to make predictions with an arbitrary length for $t > t_0$, by iteratively using Eqs. (6) and (7). Once the RC model was trained and the weights were determined, it could then be used to make predictions from any given start time. The performance of the trained model based on different strategies will be evaluated and compared in the next section.

4. Machine learning prediction

After the optimal hyper-parameters of the RC model have been determined, in this section, we evaluate the model predictions of mooring line tensions based on different strategies. Note that, for the strategies B and C, the trained model also predicts the future surge motion simultaneously. As we focus on the predictions of mooring line tension, the surge prediction will not be discussed in this work. The performances of the RC models are evaluated by comparing the tension predictions with the actual measured results from the experiments.

4.1. Prediction for the barge

First, we evaluate the mooring tension predictions of the rectangular barge given by the RC model in the test set with $t \in [11200, 13760]s$, based on three different strategies illustrated in Section 3.2. The predictions are made from 75 different initial conditions in the test set, which start from different values of t_0 as $t_0 = (11200 + 32 \times k)$ s, where k is an integer ranging from 0 to 74. The initial conditions are uniformly distributed with the interval of 100 timesteps ($\Delta t = 0.32$ s).

Fig. 15 presents some examples of the predictions of mooring line tensions F_1, F_2, F_3, and F_4 in the test set given by the RC model using different strategies. It is shown that the predictions given by the RC model based on strategy C are in the best agreement with the measured experimental results in 80 s, as the RC predictions based on strategies A and B have larger deviations. Then, the mean evaluation indexes over the test set with different prediction lengths are evaluated. Table 11 illustrates the evaluation indexes (the normalized mean absolute error E_{abs}, the extreme value error E_{max}, and the curve fitting degree R_{new}) of the RC predictions of mooring line tensions based on different strategies. In Fig. 16, the E_{abs} of predictions with different lengths based on different strategies are shown. For the prediction length of 80 s, the prediction accuracy E_{abs} of strategy B improves about 23.1% and the E_{max} improves about 16.0%, when compared with strategy A. In addition, compared with the strategy B, the strategy C can further improve the accuracy of E_{abs} about 21.5% and the E_{max} about 22.4%. It is illustrated that the RC model based on strategy C can make

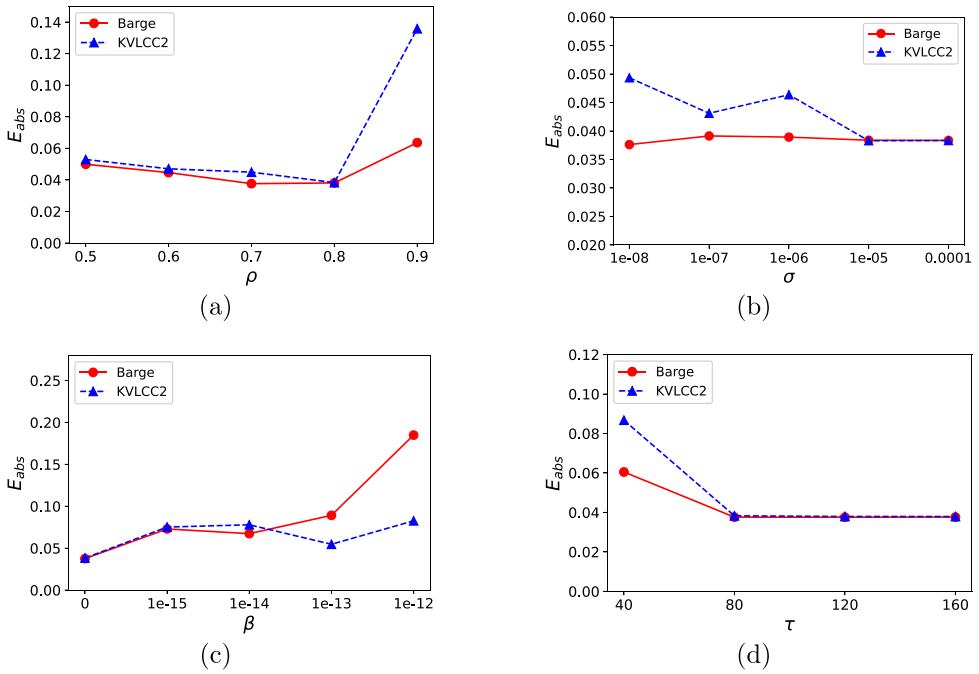

Fig. 14. Influence of hyper-parameters of the RC model on the tension predictions in the validation set based on strategy C for the barge (red) and the KVLCC2 ship (blue). (For interpretation of the references to color in this figure legend, the reader is referred to the web version of this article.)

Table 11
Evaluation indexes of predictions of mooring line tensions for the rectangular barge in the test set based on different ML strategies and models.

Prediction length	Strategy	E_{abs}	E_{max}	R_{new}
40 s	A - RC	0.0834	0.0511	0.896
	B - RC	0.0502	0.0347	0.931
	C - RC	0.0260	0.0204	0.962
	C - LSTM	0.0605	0.0443	0.919
50 s	A - RC	0.0911	0.0559	0.887
	B - RC	0.0598	0.0412	0.919
	C - RC	0.0380	0.0266	0.946
	C - LSTM	0.0710	0.0487	0.907
60 s	A - RC	0.0977	0.0588	0.879
	B - RC	0.0690	0.0466	0.908
	C - RC	0.0492	0.0351	0.930
	C - LSTM	0.0786	0.0551	0.898
70 s	A - RC	0.1020	0.0628	0.874
	B - RC	0.0754	0.0507	0.901
	C - RC	0.0572	0.0395	0.920
	C - LSTM	0.0840	0.0588	0.892
80 s	A - RC	0.1079	0.0660	0.867
	B - RC	0.0830	0.0555	0.892
	C - RC	0.0652	0.0431	0.911
	C - LSTM	0.0913	0.0627	0.883

Table 12
The computational time to train the model and to give predictions with the time interval of 80 s (250 timesteps) for the barge based on machine learning.

Barge	Strategy A - RC	Strategy B - RC	Strategy C - RC	Strategy C - LSTM
Training time	16.03 s	16.13 s	19.20 s	628.03 s
Prediction time	0.093 s	0.095 s	0.117 s	6.90 s

great predictions of mooring tensions about 80 s into the future. The normalized mean absolute error E_{abs} is 0.0652, the extreme value error E_{max} is 0.0431, and the curve fitting degree R_{new} is 0.911.

Then, we illustrate the computational time of training the RC model and using the trained model to predict mooring tension of barge based on different strategies. The training and testing for the three strategies based on the RC model were conducted on the CPU (Intel Xeon E5-2678) of the laboratory computer. The main packages used were Python 3.6 and Scikit-learn (Pedregosa et al., 2011). As shown in Table 12, the computational time of training the RC model based on strategy C with 34000 samples of data was only about 19.65 s. As the parallel computing was conducted to construct the two sub-RC models in the strategy C, the computational time of strategy C was slightly longer than that based on the strategies A and B. The computational time of the RC model based on strategy C to predict mooring line tensions of barge 80 s (250 time steps) into the future was only about 0.117 s. The accuracy of the RC model based on the strategy C was the highest among the three strategies while its computational cost of training and predicting did not increase much. Therefore, the RC model based on strategy C could be used to predict mooring line tension accurately and efficiently.

Next, we compare the performances of the RC model and the LSTM model based on the strategy C. The LSTM network is a well-known framework of RNNs. For the details about the main structure of the LSTM and the determination of its hyper-parameters for predicting the mooring tension of the barge, please refer to Appendix. The LSTM model was trained and tested on a GPU (GeForce RTX 2080 Ti) of the laboratory computer with the CPU (Intel Xeon E5-2678). The main packages used were Python 3.6 and Keras (Géron, 2022). Now we compare the RC model with the LSTM model based on the strategy C in terms of accuracy and efficiency. As shown in Fig. 15, the RC model's predictions are in better agreement with the true measurements, compared with the results given by the LSTM model. In Table 11, the evaluation indexes of mooring line tension predictions from the LSTM model are shown. In Fig. 16, the normalized absolute error E_{abs} of predictions from the LSTM model is compared with that of the RC model. It is shown that the RC model has much higher prediction accuracy compared with the LSTM model results. Besides, Table 12 compares the computational times of training and predicting for the RC model and the LSTM model. Based on strategy C, the computational time of training the LSTM model with 34000 samples of data was about 628.03 s, and the time of predicting mooring line tensions of barge 80 s (250 time steps) into the future was about 6.90 s. The RC model had much less computational time of training and predicting compared with the LSTM model.

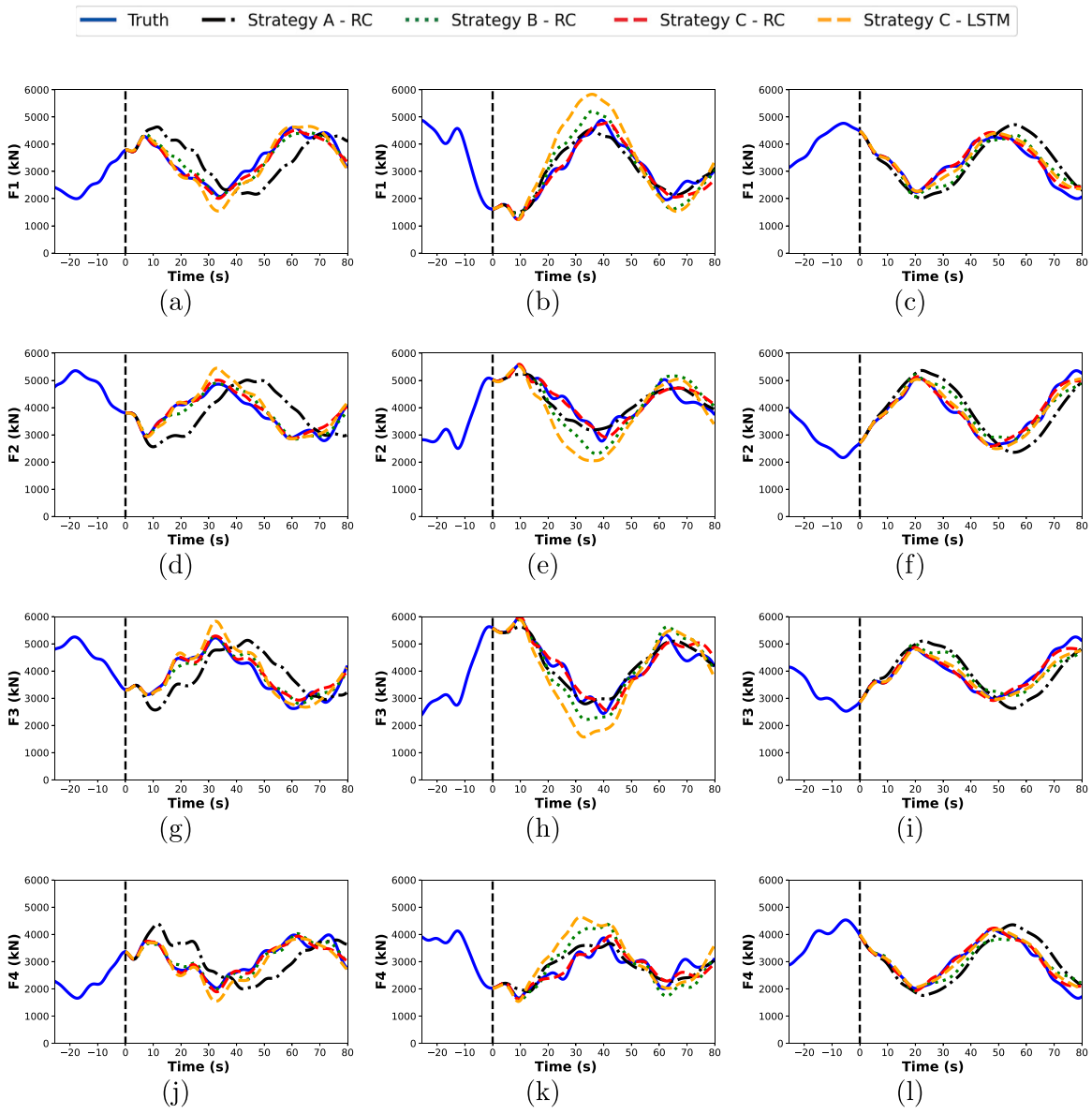

Fig. 15. Examples of mooring line tension predictions for the barge given by the ML models based on different strategies in the test set. Blue line: true measurement; Black dash-dotted line: RC model prediction based on strategy A; Green dotted line: RC model prediction based on strategy B; Red dashed line: RC model prediction based on strategy C; Orange dashed line: LSTM model prediction based on strategy C. (For interpretation of the references to color in this figure legend, the reader is referred to the web version of this article.)

The RC model based on the strategy C is effective to predict future mooring line tensions of the barge accurately. Is it possible to apply this method to other types of vessel? We will investigate the performances of ML models to predict mooring tension of the KVLCC2 ship in the following section.

4.2. Prediction for the KVLCC2 ship

Next, to test whether the ML strategy is capable of predicting mooring tension for a different type of vessel, we evaluate the ML performance for another case study of the KVLCC2 ship.

The mooring tension predictions of the KVLCC2 ship given by the ML models are evaluated in the test set with $t \in [11714, 14391]s$. The predictions are made from 75 different initial conditions in the test set, which start from different values of t_0 as $t_0 = (11714 + 33.5 \times k)$ s, where k is an integer ranging from 0 to 74. The initial conditions are uniformly distributed with the interval of 100 time steps ($\Delta t = 0.335$ s). Fig. 17 presents some examples of the predictions of mooring line tensions F_1, F_2, F_3, and F_4 in the test set given by the ML models based on different strategies. It is shown that the predictions of mooring tensions given by the RC model based on strategy C are in the best agreement with the measured results from the model test in 80 s. Then, the statistical values of the evaluation indexes in the test set are compared. Table 13 presents the evaluation indexes of the mooring tension predictions for the model test of the KVLCC2 ship based on different strategies. In Fig. 18, the normalized mean absolute errors E_{abs} of predictions with different lengths based on different strategies are shown. For the predicted length of 80 s, the prediction accuracy E_{abs} of strategy B improves about 25.5%, and the E_{max} improves about 35.8% when compared with strategy A. In addition, compared with the strategy B, the strategy C can further improve the E_{abs} about 36.5% and the E_{max} about 39.7%. In the case study of the KVLCC2 ship, it is found that the RC model based on strategy C can make great predictions of mooring tensions about 80 s into the future. The normalized mean absolute error E_{abs} is 0.0552, the extreme value error E_{max} is 0.0319, and the curve fitting degree R_{new} is 0.927. It is shown that the RC model

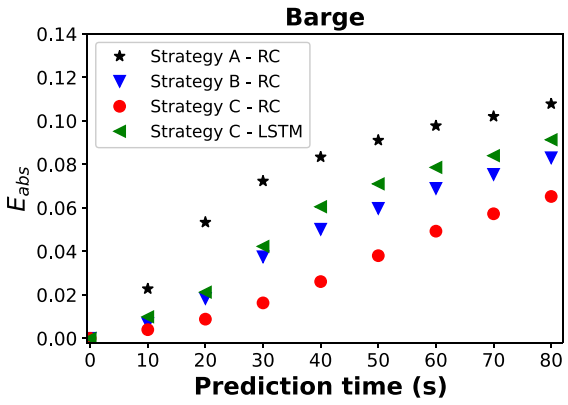

Fig. 16. The error E_{abs} of tension predictions for the barge in the test set with different prediction lengths, based on different strategies.

Table 13
Evaluation indexes of predictions of mooring line tensions for the KVLCC2 ship in the test set based on different ML strategies.

Prediction length	Strategy	E_{abs}	E_{max}	R_{new}
40 s	A - RC	0.0994	0.0603	0.888
	B - RC	0.0590	0.0395	0.931
	C - RC	0.0245	0.0187	0.970
	C - LSTM	0.0550	0.0301	0.936
50 s	A - RC	0.1021	0.0603	0.885
	B - RC	0.0647	0.0395	0.924
	C - RC	0.0293	0.0187	0.964
	C - LSTM	0.0623	0.0360	0.925
60 s	A - RC	0.1060	0.0686	0.880
	B - RC	0.0736	0.0445	0.913
	C - RC	0.0361	0.0243	0.954
	C - LSTM	0.0742	0.0450	0.910
70 s	A - RC	0.1123	0.0755	0.873
	B - RC	0.0814	0.0483	0.904
	C - RC	0.0450	0.0276	0.941
	C - LSTM	0.0861	0.0513	0.895
80 s	A - RC	0.1166	0.0811	0.868
	B - RC	0.0869	0.0529	0.898
	C - RC	0.0552	0.0319	0.927
	C - LSTM	0.0979	0.0597	0.880

Table 14
The computational time to train the model and to give predictions with the time interval of 80 s (238 time steps) for the KVLCC2 ship based on machine learning.

KVLCC2	Strategy A - RC	Strategy B - RC	Strategy C - RC	Strategy C - LSTM
Training time	16.06 s	16.18 s	19.55 s	630.82 s
Prediction time	0.090 s	0.093 s	0.106 s	6.62 s

based on strategy C is valid to predict future mooring line tensions for both two vessel types.

Then, we illustrate the computational time of training the RC model and using the trained model to predict mooring line tension based on different strategies for the KVLCC2 ship case. As shown in Table 14, the computational time of training the RC model based on strategy C with 34000 samples of data was only about 19.55 s. The computational time of the RC model based on strategy C to predict mooring line tensions of the KVLCC2 ship 80 s (238 timesteps) into the future was only about 0.106 s. The computational time was close to that of the barge case as the neuron numbers, the degree of network in the RC models, and the training samples for these two cases were the same. The RC model based on strategy C could be used to predict the mooring line tension of the KVLCC2 ship accurately and efficiently.

Then, we compare the performances of the RC model and the LSTM model based on the strategy C. The hyper-parameters of the LSTM model to predict the mooring line tension of the KVLCC2 ship are described in Appendix. As shown in Fig. 17, the RC model predictions are in better agreement with the true measurements compared with the results given by the LSTM model. The evaluation indexes of the LSTM model are shown in Table 13, and the E_{abs} of LSTM predictions with different prediction lengths are shown in Fig. 18. The comparison of training time and prediction time for the RC model and the LSTM model is shown in Table 14. It is shown that for the KVLCC2 ship case, we come to the similar conclusion that the RC model has higher accuracy and requires less computational time of training and predicting compared with the results of the LSTM model. From the investigation of the performances, it suggests that the RC model is more suitable to predict future mooring line tension compared with the LSTM network due to its higher accuracy and efficiency.

Based on the RC model, it is found that the strategy B performs better than the strategy A for making the predictions of mooring line tension. A possible explanation is that the surge motion was closely related to mooring line tension, and they had similar data structures with the low-frequency and wave-frequency parts. Including more data of the surge motion into the dataset might help the model better learn the underlying features and give better predictions of the tension. Besides, the RC model based on the strategy C has better performance compared with that based on strategy B. As the mooring line tension has the typical low-frequency and wave-frequency parts, the divided two parts might make the RC model easier learn the underlying features and better predict time series with similar frequency. The global responses would be more complex for the model to learn. Thus, it is reasonable that the RC model based on the divided frequency parts worked better. In addition, it is shown that there is no distinct difference between the accuracy of predictions for the two case studies of the barge and the KVLCC2 ship. As the RC model is data-driven, we might explain this result by analyzing their datasets. According to Figs. 12 and 13, the peak spectral periods of mooring line tension and surge motion in the barge case were all about 58.6 s, which were smaller than those in the KVLCC2 case about 84.7 s. If the significant double amplitudes of the mooring line tensions are the same, the volatility of mooring tension time series with the smaller peak spectral period could be more intense. It is likely that the time series with higher volatility would be more difficult for the ML model to learn. However, as shown in Tables 3 and 6, the mooring line tension in the barge case had a smaller significant amplitude. Taking these two factors of peak spectral period and significant wave height into account, a possible explanation is that there is no great difference in the volatility of tension for these two case studies, so the performances of the proposed method for these two case studies are similar. In the future study, a more reasonable explanation for the prediction capability of the RC model might be addressed by considering the mooring tension predictions in various case studies.

5. Concluding remarks

In this study, a machine learning (ML) approach based on the RC model is proposed to predict future mooring line tensions of floating structure. The RC model is trained based on the low-frequency and wave-frequency parts of mooring line tension combined with its main relevant vessel motion. The final prediction is obtained through the superposition of the low-frequency and wave-frequency tensions. The datasets were collected from the model tests in the deep-water wave basin to test the proposed method.

The mooring line tensions and horizontal vessel motions mainly consist of low-frequency and wave-frequency responses. As the vessels were tested in irregular head waves, the influence of surge motion on the mooring tension was much greater than that of sway and yaw motions. Therefore, the RC model was constructed based on the low-frequency and wave-frequency parts of the mooring line tension and surge motion. Finally, the trained model could provide predictions of

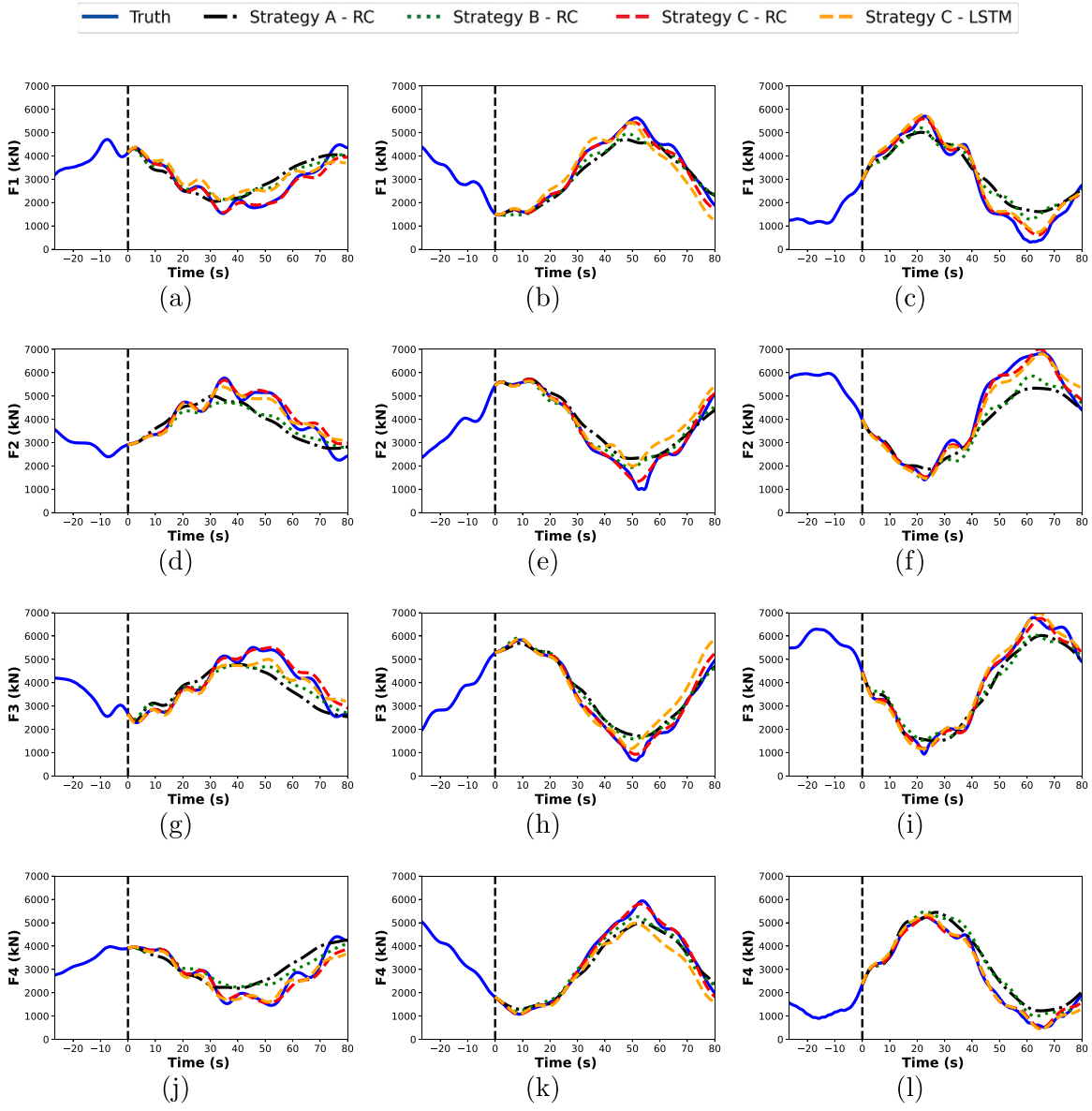

Fig. 17. Examples of mooring line tension predictions for the KVLCC2 ship given by the ML models based on different strategies in the test set. Blue line: true measurement; Black dash-dotted line: RC model prediction based on strategy A; Green dotted line: RC model prediction based on strategy B; Red dashed line: RC model prediction based on strategy C; Orange dashed line: LSTM model prediction based on strategy C. (For interpretation of the references to color in this figure legend, the reader is referred to the web version of this article.)

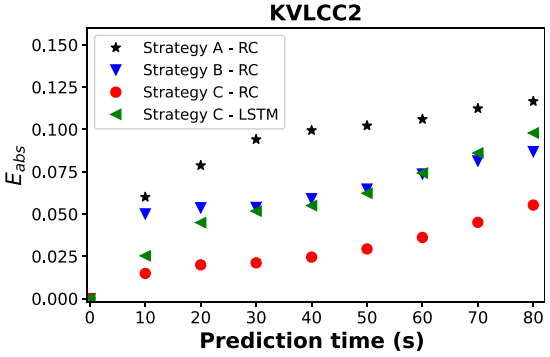

Fig. 18. The error E_{abs} of tension predictions for the KVLCC2 ship in the test set with different prediction lengths, based on different strategies.

mooring line tension 80 s into the future with high accuracy, which was validated by the corresponding experimental results.

It is illustrated that including the main relevant vessel motion into the dataset and using the divided low-frequency and wave-frequency parts to train the RC model could improve the prediction accuracy significantly. It suggests that in different offshore environments and mooring systems, we can analyze the main relevant vessel motions that contribute to the mooring line tension. Then, we combine the mooring line tension data with the main relevant vessel motion to help the RC model predict the mooring line tension accurately. What is more, the model based on the divided frequency parts could further improve prediction accuracy. Besides, compared with the LSTM model, the RC model was found to be more accurate and efficient to predict mooring tension.

This study provides some guidelines and shows the potential for applying the RC model to predict the mooring line tensions for vessels. In the present study, the training and test datasets came from one sea state for each case study of the barge and the KVLCC2 ship. The

performance of the proposed method under various sea conditions has not been investigated, as the experimental results were limited. As the sea condition is various, in the future study, the accuracy of the proposed method applied in different sea conditions needs to be further investigated, like in the well-known sea area information of the North Sea. Besides, in this work, we try to predict the mooring line tension by using the characteristic of mooring line tension that it has typical low-frequency and wave-frequency components. In terms of machine learning, it is known as a technology for estimating the field based on experience. In the future work, it could be good to think of machine learning that can be applied without this kind of academic background for predicting time series while the accuracy is maintained.

CRediT authorship contribution statement

Yu Yang: Conceptualization, Methodology, Software, Writing – original draft. **Tao Peng:** Investigation, Formal analysis, Data curation. **Shijun Liao:** Conceptualization, Methodology, Resources, Writing – review & editing.

Declaration of competing interest

The authors declare that they have no known competing financial interests or personal relationships that could have appeared to influence the work reported in this paper.

Data availability

Data will be made available on request.

Acknowledgments

We express sincere thanks to the anonymous reviewers for their valuable comments and suggestions. This work is partly supported by National Natural Science Foundation of China (No. 12272230) and Shanghai Pilot Program for Basic Research - Shanghai Jiao Tong University, China (No. 21TQ1400202).

Appendix. Long short-term memory network

In this section, we illustrate the main structure of the long short-term memory (LSTM) network. Besides, the determination of hyper-parameters of the LSTM model based on the strategy C to predict the mooring line tension is illustrated.

The LSTM recurrent network is a well-known type of RNN model. The main framework of the LSTM is a memory block consisting of a memory cell and three gates, as shown in Fig. A.1. Mathematically, the LSTM cell is described by the following core equations,

$$\boldsymbol{f}_t = \sigma(\boldsymbol{W}_f \cdot [\boldsymbol{h}_{t-1}, \boldsymbol{x}_t] + \boldsymbol{b}_f) \tag{A.1}$$

$$\boldsymbol{i}_t = \sigma(\boldsymbol{W}_i \cdot [\boldsymbol{h}_{t-1}, \boldsymbol{x}_t] + \boldsymbol{b}_i) \tag{A.2}$$

$$\tilde{\boldsymbol{c}}_t = \tanh(\boldsymbol{W}_c \cdot [\boldsymbol{h}_{t-1}, \boldsymbol{x}_t] + \boldsymbol{b}_c) \tag{A.3}$$

$$\boldsymbol{c}_t = \boldsymbol{f}_t \cdot \boldsymbol{c}_{t-1} + \boldsymbol{i}_t \cdot \tilde{\boldsymbol{c}}_t \tag{A.4}$$

$$\boldsymbol{o}_t = \sigma(\boldsymbol{W}_o[\boldsymbol{h}_{t-1}, \boldsymbol{x}_t] + \boldsymbol{b}_o) \tag{A.5}$$

$$\boldsymbol{h}_t = \boldsymbol{o}_t \cdot \tanh(\boldsymbol{c}_t), \tag{A.6}$$

where $\boldsymbol{f}_t$, $\boldsymbol{i}_t$ and $\boldsymbol{o}_t$ are the gate vector signals (forget, input and output gates), $\boldsymbol{x}_t$ is the observable input, $\boldsymbol{c}_t$ is the cell state, $\tilde{\boldsymbol{c}}_t$ is the process state, $\boldsymbol{h}_t$ is the hidden state, $\boldsymbol{W}_f, \boldsymbol{W}_i, \boldsymbol{W}_c$, and $\boldsymbol{W}_o$ are the weights, and $\boldsymbol{b}_f, \boldsymbol{b}_i, \boldsymbol{b}_c$, and $\boldsymbol{b}_o$ are the bias, and the activation function σ is sigmoid. For a detailed description of the LSTM architecture, please refer to Hochreiter and Schmidhuber (1997).

Then, we try to apply the LSTM model based on strategy C to predict the mooring line tension of the barge and the KVLCC2 ship, respectively. The determination of the hyper-parameters for the LSTM model includes the input length, the number of the LSTM layers, the number of neurons in each layer and the batch size. First, the influence of the input length was considered. The output of the LSTM network was the next step prediction. As the number of LSTM layer is ordinary less, one LSTM layer was chosen primitively. Besides, the LSTM layer was set to 128 neurons, and the batch size was 1024. The training set, validation set, and test set were the same as those illustrated in Table 8. The adaptive moment optimization (Adam) (Kingma and Ba, 2014) was applied as the optimizer, and the mean squared error was used as loss function. The training epoch was chosen as 300, because the loss values of validation set were stable when the epoch approached 300. As shown in Fig. A.2(a), the validation errors of the prediction results for different values of input length ($n = 10, 30, 50, 100, 150$) are compared. The validation error was the normalized mean absolute error of predictions with 60 s defined the same as that in the Section 3.5. The prediction of mooring line tension with the time window of inputs n equal to 100 performed the best. After the value of the input length was chosen as $n = 100$, the influence of the LSTM layer was considered. The performances of the LSTM models with different layers (one LSTM layer to four LSTM layers) were compared. According to Fig. A.2(b), the LSTM model with two layers has the minimum validation error. Then, the neuron number of each LSTM layer was further determined. In Fig. A.2(c), the predictions of the LSTM model with neuron numbers (64, 128, 256, 512) are compared. It was found that the predictions had the least error when the neuron number of each LSTM layer was equal to 128. At last, as shown in Fig. A.2, the training process with the batch size 1024 performed the best. Finally, the hyper-parameters of the LSTM model for the barge case are listed in Table A.1. When the LSTM was trained, it could be iteratively used to make future predictions.

Similarly, for the KVLCC2 ship case, the influences of input length, the number of LSTM layers, the number of neurons in each layer, and the batch size on the prediction performance are presented in Figs. A.2 (a), (b), (c) and (d), respectively. The hyper-parameter of the LSTM model for predicting the mooring line tension of the KVLCC2 is illustrated in Table A.1.

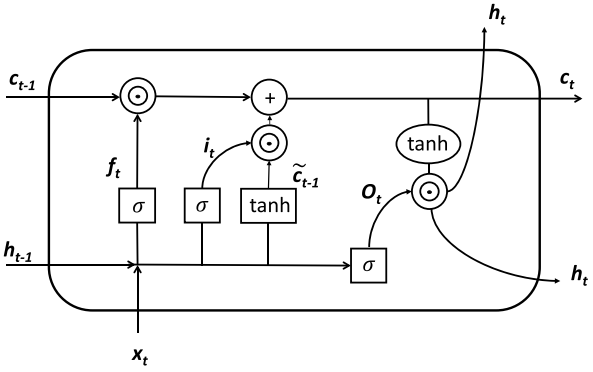

Fig. A.1. The framework of long short-term memory (LSTM) cell.

Table A.1
Hyper-parameters of the LSTM model based on strategy C for predicting the mooring line tensions of the barge and the KVLCC2 ship, respectively.

Type	Time window of inputs	LSTM layer	Neuron	Batch size	Optimizer	Epoch
Barge	100	2	128	1024	Adam	300
KVLCC2	100	2	128	1024	Adam	300

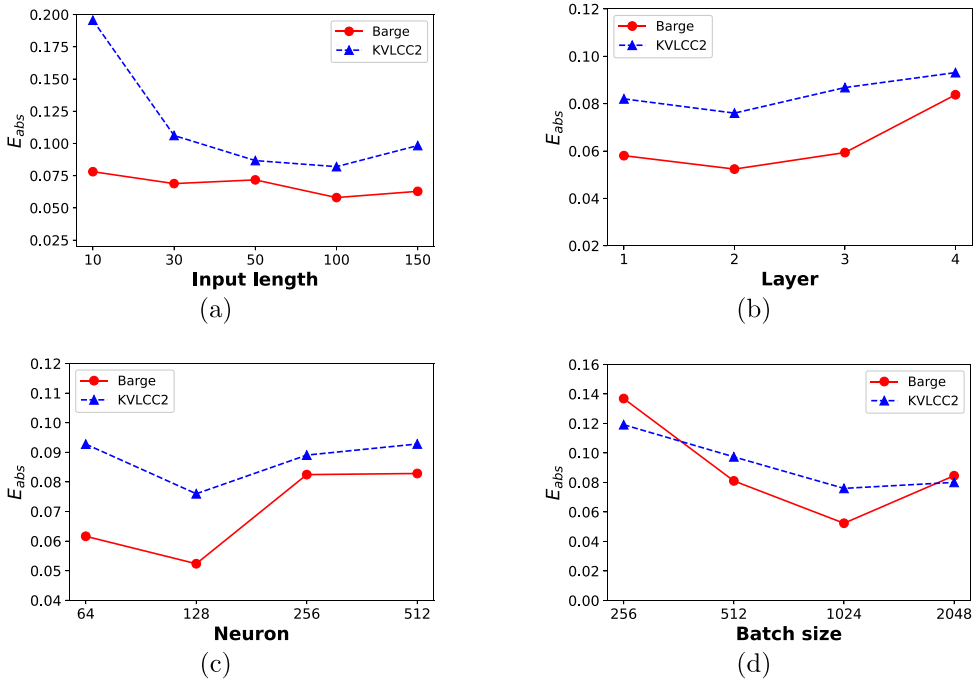

Fig. A.2. Influence of hyper-parameters of the LSTM model on the tension predictions in the validation set based on strategy C for barge (red) and KVLCC2 ship (blue). (For interpretation of the references to color in this figure legend, the reader is referred to the web version of this article.)

References

Bai, L.H., Xu, H., 2021. Accurate estimation of tidal level using bidirectional long short-term memory recurrent neural network. Ocean Eng. 235, 108765.

Bai, L.H., Xu, H., 2022. Accurate storm surge forecasting using the encoder–decoder long short term memory recurrent neural network. Phys. Fluids 34, 016601.

Chaves, V., Sagrilo, L.V., Silva, V.R.M.d., Vignoles, M.A., 2015. Artificial neural networks applied to flexible pipes fatigue calculations. In: International Conference on Offshore Mechanics and Arctic Engineering, vol. 56529. American Society of Mechanical Engineers, V05BT04A022.

Christiansen, N.H.r., Voie, P.E.T., Hø gsberg, J., 2015. Artificial neural networks for reducing computational effort in active truncated model testing of mooring lines. In: International Conference on Offshore Mechanics and Arctic Engineering, vol. 56475. American Society of Mechanical Engineers, V001T01A018.

De Girolamo, P., Crespi, M., Romano, A., Mazzoni, A., Di Risio, M., Pasquali, D., Bellotti, G., Castellino, M., Sammarco, P., 2019. Estimation of wave characteristics based on global navigation satellite system data installed on board sailboats. Sensors 19, 2295.

Géron, A., 2022. Hands-on Machine Learning with Scikit-Learn, Keras, and TensorFlow. O'Reilly Media, Inc..

Guo, X., Zhang, X., Tian, X., Li, X., Lu, W., 2021. Predicting heave and surge motions of a semi-submersible with neural networks. Appl. Ocean Res. 112, 102708.

Guo, X., Zhang, X., Tian, X., Lu, W., Li, X., 2022. Probabilistic prediction of the heave motions of a semi-submersible by a deep learning model. Ocean Eng. 247, 110578.

Hochreiter, S., Schmidhuber, J., 1997. Long short-term memory. Neural Comput. 9, 1735–1780.

Jaeger, H., Haas, H., 2004. Harnessing nonlinearity: Predicting chaotic systems and saving energy in wireless communication. Science 304, 78–80.

Janas, K., Milne, I., Whelan, J., 2021. Application of a convolutional neural network for mooring failure identification. Ocean Eng. 232, 109119.

Jiang, J., Lai, Y.-C., 2019. Model-free prediction of spatiotemporal dynamical systems with recurrent Neural Network: Role of network spectral radius. Phys. Rev. Res. 1, 033056.

Jordan, M.I., Mitchell, T.M., 2015. Machine learning: Trends, perspectives, and prospects. Science 349, 255–260.

Kim, Y., 2015. Prediction of the dynamic response of a slender marine structure under an irregular ocean wave using the NARX-based quadratic Volterra series. Appl. Ocean Res. 49, 42–56.

Kingma, D.P., Ba, J., 2014. Adam: A method for stochastic optimization. arXiv preprint arXiv:1412.6980.

Kumar, N., Liong, C.T., Chen, W.K., Magee, A.R., Chua, K.H., Choo, Y.S., 2020. Development of data-driven models for prediction of mooring line tensions. In: International Conference on Offshore Mechanics and Arctic Engineering, vol. 84317. American Society of Mechanical Engineers, V001T01A011.

Li, J., Cao, Z., Borthwick, A.G., 2021a. Uncertainty quantification in shallow water-sediment flows: A stochastic Galerkin shallow water hydro-sediment-morphodynamic model. Appl. Math. Model. 99, 458–477.

Li, X., Gu, J., Yao, Z., 2021b. Numerical study on the hydrodynamics of tuna morphing median fins during C-turn behaviors. Ocean Eng. 236, 109547.

Liong, C., Chua, K., 2022. Data assimilation for deterministic prediction of vessel motion in real-time. Ocean Eng. 244, 110356.

Lu, Z., Hunt, B.R., Ott, E., 2018. Attractor reconstruction by machine learning. Chaos 28, 061104.

Ma, K.T., Luo, Y., Kwan, C.-T.T., Wu, Y., 2019. Mooring System Engineering for Offshore Structures. Gulf Professional Publishing.

Mak, B., Düz, B., 2019. Ship as a wave buoy: Estimating relative wave direction from in-service ship motion measurements using machine learning. In: International Conference on Offshore Mechanics and Arctic Engineering, vol. 58882. American Society of Mechanical Engineers, V009T13A043.

Mandic, D., Chambers, J., 2001. Recurrent Neural Network for Prediction: Learning Algorithms, Architectures and Stability. Wiley.

Mikolov, T., Karafiát, M., Burget, L., Cernockỳ, J., Khudanpur, S., 2010. Recurrent neural network based language model. In: Interspeech, vol. 2. Makuhari, pp. 1045–1048.

Mitchell, T.M., Mitchell, T.M., 1997. Machine Learning, vol. 1. McGraw-hill New York.

Nakai, K., Saiki, Y., 2018. Machine-learning inference of fluid variables from data using reservoir computing. Phys. Rev. E 98, 023111.

Pathak, J., Hunt, B., Girvan, M., Lu, Z., Ott, E., 2018. Model-free prediction of large spatiotemporally chaotic systems from data: A reservoir computing approach. Phys. Rev. Lett. 120, 024102.

Pathak, J., Lu, Z., Hunt, B.R., Girvan, M., Ott, E., 2017. Using machine learning to replicate chaotic attractors and calculate Lyapunov exponents from data. Chaos 27, 121102.

Pedregosa, F., Varoquaux, G., Gramfort, A., Michel, V., Thirion, B., Grisel, O., Blondel, M., Prettenhofer, P., Weiss, R., Dubourg, V., et al., 2011. Scikit-learn: Machine learning in Python. J. Mach. Learn. Res. 12, 2825–2830.

Qiao, D., Li, P., Ma, G., Qi, X., Yan, J., Ning, D., Li, B., 2021. Realtime prediction of dynamic mooring lines responses with LSTM neural network model. Ocean Eng. 219, 108368.

Quéau, L.M., Kimiaei, M., Randolph, M.F., 2014. Artificial neural network development for stress analysis of steel catenary risers: sensitivity study and approximation of static stress range. Appl. Ocean Res. 48, 148–161.

Rezaniaiee Aqdam, H., Ettefagh, M.M., Hassannejad, R., 2018. Health monitoring of mooring lines in floating structures using artificial neural networks. Ocean Eng. 164, 284–297.

Sclavounos, P.D., Ma, Y., 2018. Artificial intelligence machine learning in marine hydrodynamics. In: International Conference on Offshore Mechanics and Arctic Engineering, vol. 51302. American Society of Mechanical Engineers, V009T13A028.

Sidarta, D.E., Kyoung, J., O'Sullivan, J., Lambrakos, K.F., 2017. Prediction of offshore platform mooring line tensions using artificial neural network. In: International Conference on Offshore Mechanics and Arctic Engineering, vol. 57632. American Society of Mechanical Engineers, V001T01A079.

Tanaka, G., Yamane, T., Héroux, J.B., Nakane, R., Kanazawa, N., Takeda, S., Numata, H., Nakano, D., Hirose, A., 2019. Recent advances in physical reservoir computing: A review. Neural Netw. 115, 100–123.

Tikhonov, A.N., Arsenin, V.Y., 1977. Solutions of Ill-Posed Problems, vol. 1. New York, p. 30.

Vlachas, P.R., Pathak, J., Hunt, B.R., Sapsis, T.P., Girvan, M., Ott, E., Koumoutsakos, P., 2020. Backpropagation algorithms and reservoir computing in recurrent Neural Network for the forecasting of complex spatiotemporal dynamics. Neural Netw. 126, 191–217.

Wang, Z., Qiao, D., Yan, J., Tang, G., Li, B., Ning, D., 2022. A new approach to predict dynamic mooring tension using LSTM neural network based on responses of floating structure. Ocean Eng. 249, 110905.

Xiao, L., Tao, L., Yang, J., Li, X., 2014. An experimental investigation on wave runup along the broadside of a single point moored FPSO exposed to oblique waves. Ocean Eng. 88, 81–90.

Yan, Z., Liu, Z., Li, Y., 2020. Numerical simulations of collinear finite amplitude steady-state resonant waves in deep water. Ocean Eng. 212, 107703.

Yang, X., Li, Y., 2022. On bi-chromatic steady-state gravity waves with an arbitrary included angle. Phys. Fluids 34, 032107.

Yang, Y., Peng, T., Liao, S., 2022. Predicting 3-DoF motions of a moored barge by machine learning. J. Ocean Eng. Sci. http://dx.doi.org/10.1016/j.joes.2022.08.001.